Demixing light paths inside disordered metamaterials

I. M. Vellekoop[1], **E. G. van Putten**[1], **A. Lagendijk**[1,2] **and A. P. Mosk**[1]

[1]*Complex Photonic Systems, Faculty of Science and Technology and MESA*$^+$ *Institute for Nanotechnology, University of Twente, P.O.Box 217, 7500 AE Enschede, The Netherlands*
[2]*FOM Institute for Atomic and Molecular Physics, Kruislaan 407, 1098 SJ Amsterdam, The Netherlands*
i.m.vellekoop@utwente.nl

http://cops.tnw.utwente.nl

Abstract: We experimentally demonstrate the first method to focus light inside disordered photonic metamaterials. In such materials, scattering prevents light from forming a geometric focus. Instead of geometric optics, we used multi-path interference to make the scattering process itself concentrate light on a fluorescent nanoscale probe at the target position. Our method uses the fact that the disorder in a solid material is fixed in time. Therefore, even disordered light scattering is deterministic. Measurements of the probes fluorescence provided the information needed to construct a specific linear combination of hundreds of incident waves, which interfere constructively at the probe.

OCIS codes: (160.3918) Metamaterials; (290.4210) Multiple scattering; (290.1990) Diffusion; (030.6600) Statistical Optics

References and links

1. U. Leonhardt, "Optical Conformal Mapping," Science **312**, 1777–1780 (2006).
2. J. B. Pendry, D. Schurig, and D. R. Smith, "Controlling Electromagnetic Fields," Science **312**, 1780–1782 (2006).
3. T. Yoshie, A. Scherer, J. Hendrickson, G. Khitrova, H. M. Gibbs, G. Rupper, C. Ell, O. B. Shchekin, and D. G. Deppe, "Vacuum Rabi splitting with a single quantum dot in a photonic crystal nanocavity," Nature **432**, 200–203 (2004).
4. H. J. Lezec, J. A. Dionne, and H. A. Atwater, "Negative Refraction at Visible Frequencies," Science **316**, 430–432 (2007).
5. G. Dolling, M. Wegener, C. M. Soukoulis, and S. Linden, "Negative-index metamaterial at 780 nm wavelength," Opt. Lett. **1**, 53–55 (2007).
6. V. M. Shalaev, "Optical negative-index metamaterials," Nature Photonics **1**, 41–48 (2007).
7. V. G. Veselago, "The electrodynamics of substances with simultaneously negative values of ε and μ," Sov. Phys. Usp. **10**, 509 (1968).
8. Z. Liu, H. Lee, Y. Xiong, C. Sun, and X. Zhang, "Far-Field Optical Hyperlens Magnifying Sub-Diffraction-Limited Objects," Science **315**, 1686 (2007).
9. G. Lerosey, J. de Rosny, A. Tourin, and M. Fink, "Focusing Beyond the Diffraction Limit with Far-Field Time Reversal," Science **315**, 1120–1122 (2007).
10. M. Baudrier-Raybaut, R. Haidar, P. Kupecek, P. Lemasson, and E. Rosencher, "Random quasi-phase-matching in bulk polycrystalline isotropic nonlinear materials," Nature **432**, 374–376 (2004).
11. M. I. Stockman, D. J. Bergman, C. Anceau, S. Brasselet, and J. Zyss, "Enhanced Second-Harmonic Generation by Metal Surfaces with Nanoscale Roughness: Nanoscale Dephasing, Depolarization, and Correlations," Phys. Rev. Lett. **92**, 057402 (2004).
12. C. W. J. Beenakker, "Random-matrix theory of quantum transport," Rev. Mod. Phys. **69**, 731–808 (1997).
13. J. B. Pendry, A. MacKinnon, and P. J. Roberts, "Universality Classes and Fluctuations in Disordered Systems," Proc. R. Soc. Lond. A **437**, 67–83 (1992).

#89796 - $15.00 USD Received 15 Nov 2007; revised 20 Dec 2007; accepted 21 Dec 2007; published 2 Jan 2008

14. P. Lodahl, A. P. Mosk, and A. Lagendijk, "Spatial Quantum Correlations in Multiple Scattered Light," Phys. Rev. Lett. **95**, 173901 (2005).
15. M. Störzer, P. Gross, C. M. Aegerter, and G. Maret, "Observation of the Critical Regime Near Anderson Localization of Light," Phys. Rev. Lett. **96**, 063904 (2006).
16. S. Zhang, B. Hu, P. Sebbah, and A. Z. Genack, "Speckle Evolution of Diffusive and Localized Waves," Phys. Rev. Lett. **99**, 063902 (2007).
17. P. Sebbah, B. Hu, A. Z. Genack, R. Pnini, and B. Shapiro, "Spatial-field correlation: The building block of mesoscopic fluctuations," Phys. Rev. Lett. **88**(12), 123901 (2002).
18. T. Schwartz, G. Bartal, S. Fishman, and M. Segev, "Transport and Anderson localization in disordered two-dimensional photonic lattices," Nature **446**, 52–55 (2007).
19. Y. A. Vlasov, V. N. Astratov, A. V. Baryshev, A. A. Kaplyanskii, O. Z. Karimov, and M. F. Limonov, "Manifestation of intrinsic defects in optical properties of self-organized opal photonic crystals," Phys. Rev. E **61**, 5784–5793 (2000).
20. S. Hughes, L. Ramunno, J. F. Young, and J. E. Sipe, "Extrinsic Optical Scattering Loss in Photonic Crystal Waveguides: Role of Fabrication Disorder and Photon Group Velocity," Phys. Rev. Lett. **94**, 033903 (2005).
21. A. F. Koenderink, A. Lagendijk, and W. L. Vos, "Optical extinction due to intrinsic structural variations of photonic crystals," Phys. Rev. B **72**, 153102 (2005).
22. R. K. Tyson, *Principles of Adaptive Optics*, 2nd ed. (Academic Press, 1998).
23. F. Roddier (ed.), *Adaptive Optics in Astronomy*, (Cambridge University Press, U.S., 1997).
24. "Special Issue: Advances in Retinal Imaging", J. Opt. Soc. Am. A 24, 1223–1480 (2007)
25. A. M. Weiner, "Femtosecond pulse shaping using spatial light modulators" Rev. Sci. Instrum. **71** 1929–1960 (2000).
26. M. Fink, D. Cassereau, A. Derode, C. Prada, P. Roux, M. Tanter, J.-L. Thomas, and F. Wu, "Time-reversed acoustics," Rep. Prog. Phys. **63**, 1933–1995 (1999).
27. R. A. Fisher, ed., *Optical phase conjugation* (Academic Press, 1983).
28. I. M. Vellekoop and A. P. Mosk, "Focusing coherent light through opaque strongly scattering media," Opt. Lett. **32**, 2309–2311 (2007).
29. M. Han, X. Gao, J. Z. Su, and S. Nie, "Quantum-dot-tagged microbeads for multiplexed optical coding of biomolecules," Nature Biotech. **19**, 631–635 (2001).
30. S. John and R. Rangarajan, "Optimal structures for classical wave localization: an alternative to the ioffe-regel criterion," Phys. Rev. B **38**, 10101 – 10104 (1988).
31. N. M. Shapiro, M. Campillo, L. Stehly, and M. H. Ritzwoller, "High-Resolution Surface-Wave Tomography from Ambient Seismic Noise," Science **307**, 1615 (2005).
32. R. L. Weaver and O. I. Lobkis, "Fluctuations in diffuse field-field correlations and the emergence of the Greens function in open systems," J. Acoust. Soc. Am. **117**, 3432–3439 (2005).
33. We thank Carlo Beenakker and John Pendry for discussions on this promising field.
34. E. G. van Putten, I. M. Vellekoop, and A. P. Mosk, "Spatial amplitude and phase modulation using commercial twisted nematic LCDs," ArXiv.org:physics.optics/0711.4301 (2007).
35. J. G. Rivas, R. Sprik, C. M. Soukoulis, K. Busch, and A. Lagendijk, "Optical transmission through strong scattering and highly polydisperse media," Europhys. Lett. **48**, 22–28 (1999).
36. M. U. Vera and D. J. Durian, "Angular distribution of diffusely transmitted light," Phys. Rev. E **53**, 3215–3224 (1996).
37. A. S. McLean and J. B. Pendry, "Beyond Diffusion to Diffraction," J. Mod. Opt. **42**, 2495–2531 (1995).
38. H. S. Carslaw and J. C. Jaeger, *Conduction of heat in solids*, 2nd ed. (University Press, Oxford, 1959).
39. S. Chandrasekhar, *Radiative Transfer* (Dover Publications, Inc., New York, 1960).
40. J. W. Goodman, *Statistical optics* (Wiley, New York, 2000).
41. N. Garcia and A. Z. Genack, "Crossover to strong intensity correlation for microwave radiation in random media," Phys. Rev. Lett. **63**, 1678–1681 (1989).
42. A. D. Mirlin, R. Pnini, and B. Shapiro, "Intensity distribution for waves in disordered media: Deviations from Rayleigh statistics," Phys. Rev. E **57**, R6285–R6288 (1998).
43. B. A. van Tiggelen, A. Tip, and A. Lagendijk, "Dwell times for light and electrons," J. Phys. A **26**, 1731–1748 (1993).
44. J. F. de Boer, *Optical fluctuations on the transmission and reflection of mesoscopic systems* (University of Amsterdam, Amsterdam, 1995).
45. E. Akkermans, P. E. Wolf, and R. Maynard, "Coherent Backscattering of Light in Disordered Media: Analysis of the Peak Line Shape," Phys. Rev. Lett. **56**, 1471–1474 (1986).

Photonic metamaterials are materials that gain their optical properties from their nanostructure, rather than from their chemical composition. Their sub-wavelength elements interact very strongly with the electromagnetic field and provide unprecedented control over the propagation of light [1, 2]. Exciting perspectives of metamaterials include field enhancement in photonic

#89796 - $15.00 USD Received 15 Nov 2007; revised 20 Dec 2007; accepted 21 Dec 2007; published 2 Jan 2008

crystal cavities [3], negative refractive index optics [4–6], and sub-wavelength imaging [7, 8]. Perhaps even more amazing is the use of metamaterials to cloak objects, making them completely invisible for a certain frequency of light [1, 2]. While these perspectives require near-perfectly manufactured metamaterials, intentionally disordered metamaterials also find applications such as sub-wavelength focusing [9] and enhanced non-linear conversion [10, 11]. Furthermore, disordered metamaterials are of fundamental interest because of their analogy to electrical conductors [12, 13], their quantum optical properties [14], and mesoscopic transport phenomena [15–17]. Recently it was shown experimentally that localization induced by disorder can confine and guide light [18].

To direct light to a desired position in a metamaterial requires thorough knowledge of the propagation of light in these structures. Since metamaterials are strongly photonic, even weak manufacturing imperfections strongly influence propagation [19–21], which makes it even harder to get light to the right place. For disordered metamaterials it is, even in theory, impossible to have *a priori* knowledge of light propagation. To treat the metamaterial as a homogeneous medium and pretend to focus somewhere inside (Fig. 1(a)) is an erroneous approach; in reality, the structure of the material prevents light from forming any focus at all.

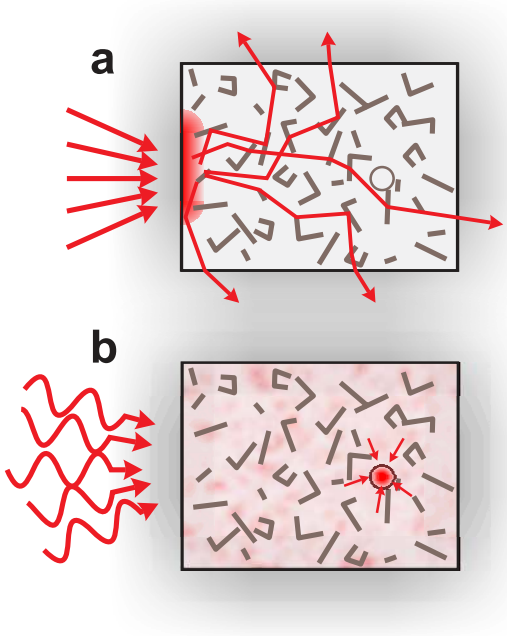

Fig. 1. Principle of channel demixing. (a) Conventional way of illuminating a metamaterial sample or device. In order to get light to the area inside the metamaterial indicated by the circle, one might try to focus light using an ordinary lens. However, the randomly oriented nanoparticles in the material mix the incident scattering channels in a complicated way so that light does not travel directly to the target. Incident rays will not converge to a geometrical focus. (b) Our new way of illuminating a specific point inside a metamaterial. The wave nature of light is used as an advantage. When the phase delay for each of the incident scattering channels is set correctly, the channels demix inside the sample; multi-channel interference makes the light focus at the desired point.

We demonstrate experimentally that light can be delivered to a target inside a disordered photonic metamaterial, or in fact any strongly scattering solid, without having any *a priori*

#89796 - $15.00 USD Received 15 Nov 2007; revised 20 Dec 2007; accepted 21 Dec 2007; published 2 Jan 2008

knowledge of the optical properties of the system. Our approach is based on the fact that the structure of the metamaterial mixes light entering through different scattering channels (a scattering channel is an angular or spatial mode of the optical field [12]). The mixing process is complex and stochastic due to disorder. Even so, reciprocity dictates that there always exists a linear combination of incident channels that demix inside the metamaterial to focus at the target. In our experiment we find this unique configuration and focus light on a target that is deeply embedded in a disordered photonic structure (Fig. 1(b)).

It is well known that the inverse wave problem is ill posed. In other words, even in principle optical measurements cannot be used to reconstruct the three-dimensional structure of a photonic metamaterial. Likewise, optical reflection and transmission measurements cannot reveal the combination of channels that demix inside the material.

There exist different methods for focusing waves in the presence of scattering. In transparent media where geometrical optics applies, delivery of light can be achieved very effectively using a variety of adaptive optics wavefront correction techniques (see e.g. Ref. 22). For example, adaptive optics is commonly used to reduce astronomical seeing [23], to improve the resolution of ophthalmic imaging [24], or for femtosecond pulse shaping [25]. Unfortunately, these adaptive optics techniques break down in nanostructured media where geometrical optics is not applicable.

For ultrasound and microwaves time-reversal has proven highly effective [9,26] in refocusing waves. Lightwaves can be refocused back to their source by phase conjugation [27], or they can be focused behind a scattering region by using feedback from an external detector [28]. All these methods require physical access to the target position, to place a transceiver, an extensive non-linear medium, or a detector. Inside a photonic metamaterial, with structures smaller than the wavelength of light, these methods cannot be used.

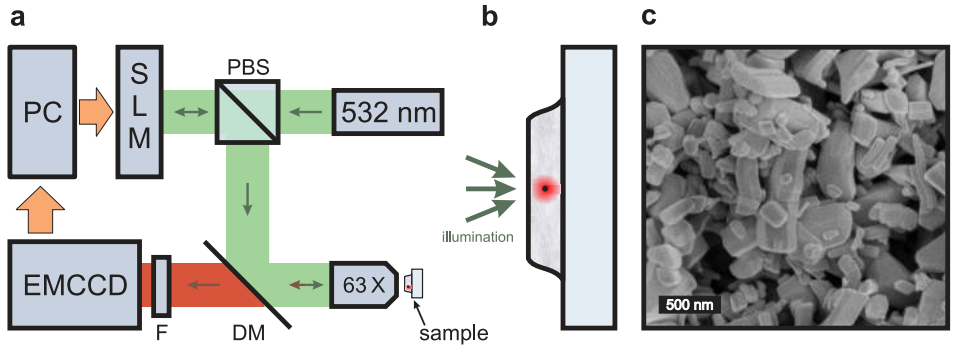

Fig. 2. Experimental setup and samples. (a) Simplified schematic of the experiment. A 532 nm laser is expanded and illuminates a spatial light modulator (SLM) that spatially modulates the phase of the reflected light. The SLM is imaged onto the back aperture of a 63x microscope objective that focuses the modulated light on a sample. Fluorescence light is collected by the same objective and imaged with an EMCCD camera. A computer drives the SLM and analyzes the EMCCD images. PBS, polarizing beam splitter. DM, dichroic mirror. F, fluorescence filter. Lenses were omitted from the schematic. (b) Geometry of the samples. A low concentration of 300-nm diameter fluorescent spheres is dispersed in a zinc oxide pigment, deposited on a glass substrate. (c) SEM image of a sample.

We have developed an approach that does allow focusing of light inside a metamaterial. Our method combines an advanced feedback and control system with a nanoscale fluorescent probe that is situated at the desired location. The power of the emitted light is a measure for the intensity at the position of the probe. In our experiment (Fig. 2(a)), we used a liquid crystal spatial

#89796 - $15.00 USD Received 15 Nov 2007; revised 20 Dec 2007; accepted 21 Dec 2007; published 2 Jan 2008

light modulator (SLM) that spatially modulates the phase of light coming from a green (532 nm) continuous wave laser. The pixels of the SLM are grouped into 640 square segments that are imaged onto the back aperture of a microscope objective. In this configuration, at the focal plane of the objective each segment corresponds to a solid angle encompassing approximately one mesoscopic scattering channel. For each of these incoming channels the phase can be set individually using the SLM. The microscope objective illuminates a sample that is mounted on a xyz-translation stage. The fluorescence light emitted by the probe inside the sample is collected by the same microscope objective and imaged with an electron multiplying charge coupled device (EMCCD) camera placed in a confocal reflection configuration. Our samples consist of a white layer of zinc oxide (ZnO) pigment on a glass substrate (Fig. 2(b)). The pigment grains have an average diameter of 200 nm, resulting in a sub-wavelength disordered structure (Fig. 2(c)). The pigment layer is up to 32 μm thick, and all samples are fully opaque. The transport mean free path was measured by fully analyzing transport of light through a series of samples (See Appendix A. The samples were found to be strongly photonic with a mean free path of 0.7 ± 0.2 μm, comparable to the wavelength of light. Fluorescent spheres with a diameter of 300 ± 15 nm are sparsely dispersed through the sample.

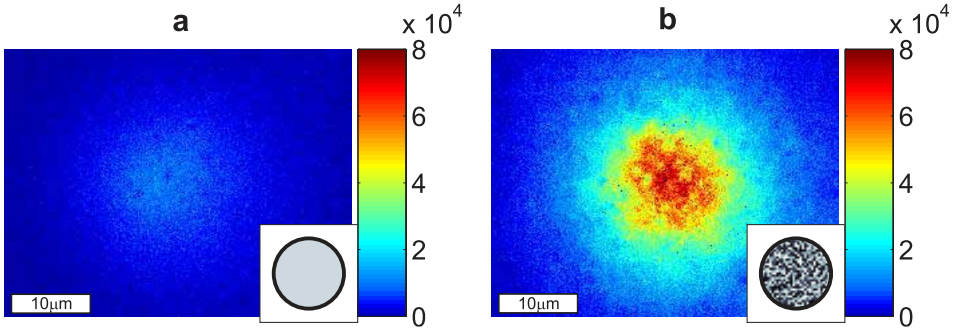

Fig. 3. Experimental demonstration of channel demixing. (a) Fluorescence image of a 300 nm sphere, embedded in ZnO pigment at a depth of 9.7 μm. Conventional illumination after a scan to find the position where the fluorescence is maximal; approximately 3 times the speckle average intensity. Inset, phase of the incident wavefront (plane wave). (b) Our channel demixing method. Same sphere and sample position as in (a), the phases of the incident channels were set to the measured optimal values. The resulting fluorescence intensity has increased by a factor of 22 with respect to the average intensity. Inset, phase of the incident wavefront. Inside the sample this seemingly random wavefront transforms into a focus. Intensities are in counts per second.

Conventional focusing of light does not work in disordered photonic media. The absence of a ballistic focus was confirmed by performing an extensive 3-dimensional scan of the sample with respect to the microscope objective (See Appendix A). The only change in the fluorescence emission was the result of the volume speckle field in the medium that is formed by scattered monochromatic light. As the sample moves, the weak fluorescence emission fluctuates randomly with the sample position. We consequently find that the maximal emission found by scanning the sample is only approximately 3 times the typical emission. In numerical simulations we find a similarly weak enhancement (Appendix B). The fluorescence emission with the sample positioned at the brightest speckle is shown in Fig. 3(a).

We now cycle the relative phase of a single incident channel between 0 and 2π while keeping the phase of all other channels constant. The intensity at the probe is the result of interference between the modulated channel and the other channels, and therefore has a sinusoidal dependence on the phase. From the phase and the amplitude of the sinusoid we obtain the complex

#89796 - $15.00 USD Received 15 Nov 2007; revised 20 Dec 2007; accepted 21 Dec 2007; published 2 Jan 2008

propagation amplitude from the modulated channel to the point inside the metamaterial. The complete set of propagation amplitudes contains all information that is needed to calculate the propagation of any incident wave towards the target. The optimal configuration of incident channels is found by taking the complex conjugate of the propagation amplitudes, so as to fully compensate for the mixing of the channels that will occur.

Figure 3(b) shows the strong increase in fluorescence emission that was achieved with channel demixing. By constructing the optimal configuration of incident channels, the intensity distribution inside the sample changed from random speckle to a pattern specially tailored for focusing light at the target. We find that the amplitudes for neighboring channels were uncorrelated, which is an indication that the channels were originally fully mixed. Light from different incident channels mixed while propagating in the medium and demixed again at the target position to form a focus. This focus was a factor of 22 more intense than the typical intensity and a factor of 6 more intense than the maximum that was achieved by searching for the brightest speckle.

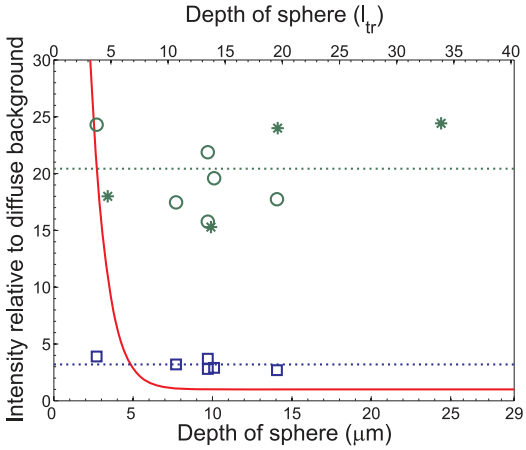

Fig. 4. Measured intensity for targets at different depths inside a 29 ± 3 μm thick sample. Stars (green), results of our channel demixing technique, starting from a random sample position. An intensity was reached that is on average 20.4 times higher than the diffuse background (green dotted line). Circles (green), results of our channel demixing technique starting on a bright speckle, demonstrating that starting from a bright spot is not advantageous. Squares (blue), maximum intensity that was achieved by searching for the brightest speckle. An average intensity increase of only 3.2 was obtained (blue dotted line). Solid line (red), theoretical best case speckle average using adaptive optics, assuming that all geometrical aberrations are corrected perfectly. All measurements are normalized to the diffuse background.

The experiment was repeated for targets at different depths inside a 29 ± 3 μm thick sample. In Fig. 4 the target intensity that was reached with channel demixing is compared to the maximum intensity reached by translating the sample. Channel demixing increases the intensity at the target by a factor of on average 20.4, regardless of the depth of the target. It makes no difference whether the sample was meticulously placed on the brightest speckle first or whether the channel demixing procedure was started without a preceding scan of the sample position. For completeness, we also plot the calculated residual ballistic focusing component that can be expected when the sphere is placed exactly in the geometrical focus. For this calculation, we optimistically assumed that all geometric aberrations are perfectly corrected by an adaptive optics system [22]. As can be seen in Fig. 4, adaptive optics could be effective for targets that are

#89796 - $15.00 USD Received 15 Nov 2007; revised 20 Dec 2007; accepted 21 Dec 2007; published 2 Jan 2008

only a few mean free paths deep. When the target lies deeper, scattering on the sub-wavelength structure of the material destroys even a perfectly corrected geometrical focus. Using channel demixing, however, we consequently find that the increase does not depend on the position of the target. Therefore, we conclude that scattering in no way limits the depth at which light can be delivered inside the metamaterial.

Theoretically, in the current experimental configuration, channel demixing has the possibility to achieve an intensity ratio that is approximately four times as high as the measured value of 20.4 (See Appendix B). In practice, however, we are limited by photobleaching of the probe. We expect to achieve even higher intensity ratios as more stable probes, such as quantum dot assemblies [29], become available.

The measured set of complex propagation amplitudes characterizes propagation of light towards a sub-wavelength target inside the metamaterial. For this measurement no physical access to the target is required; it is not even required to know where the target probe exactly is. In both ordered and disordered metamaterials these amplitudes contain information about the structure and the optical quality of the metamaterial [20, 30–32]. This information, which was not experimentally accessible before, makes channel demixing a unique method for characterizing any metamaterial. Our experimental results call for the development of theoretical approaches that treat light propagation inside disordered photonic metamaterials [33].

We have shown that light can be focused on a target inside a photonic metamaterial that completely scrambles the incident waves. Since the illumination is selective, channel demixing can be used to increase the contrast with a fluorescent background. A different application would be to selectively activate photochemical processes by concentrating light at a point inside a scattering material. Finally, the use of a fluorescent probe permits selectively focusing light on fluorescent areas, which is highly desirable in biological imaging, and may be a key technology for selectively illuminating individual cells in disordered biomaterials such as human skin tissue.

A. Experimental details

A.1. Apparatus

The goal of the experiment is to illuminate a disordered medium in such a way that light focuses at a predefined target deep inside. The experimental setup consists of a spatial light modulator that is used to adjust the illumination, and a confocal fluorescence microscope that indirectly measures the intensity at the target. A detailed schematic of the setup is given in Fig. 5. Light from a continuous wave 532 nm laser (Coherent Compass M315-100) is expanded using a 30x beam expander. The expanded beam illuminates a Holoeye LC-R 2500 spatial light modulator (SLM) with a resolution of 1024 x 768 pixels. The pixels are grouped into square segments of 20 x 20 pixels. We have independent control over the phase and amplitude of each of the segments [34]. During this experiment, the amplitude of all segments is kept constant. The SLM is imaged onto the back aperture of a microscope objective using a 1:2 demagnifying telescope. In total, 640 segments fall within the aperture of the objective, which means that we control 640 degrees of freedom. The microscope objective (Zeiss infinity corrected 63x, NA=0.95 Achroplan air) focuses the light on the sample, thereby mapping the segments to channels in k-space. The sample is mounted on a XYZ-nanopositioning stage (Physik Instrumente P-611.3S NanoCube) to allow for a precise 3D-scan of the geometrical focus.

The returned fluorescence light is separated from the excitation light using a combination of a dichroic mirror (Semrock FF562-Di02-25x36) and a bandpass filter (Semrock FF01-593/40-25). An electron multiplying CCD camera (Andor Luca DL-658M) images the fluorescence emission. A computer sums the intensity in the camera image to find the total power in the diffuse spot of fluorescence light. For each of the segments, measurements are performed at

#89796 - $15.00 USD Received 15 Nov 2007; revised 20 Dec 2007; accepted 21 Dec 2007; published 2 Jan 2008

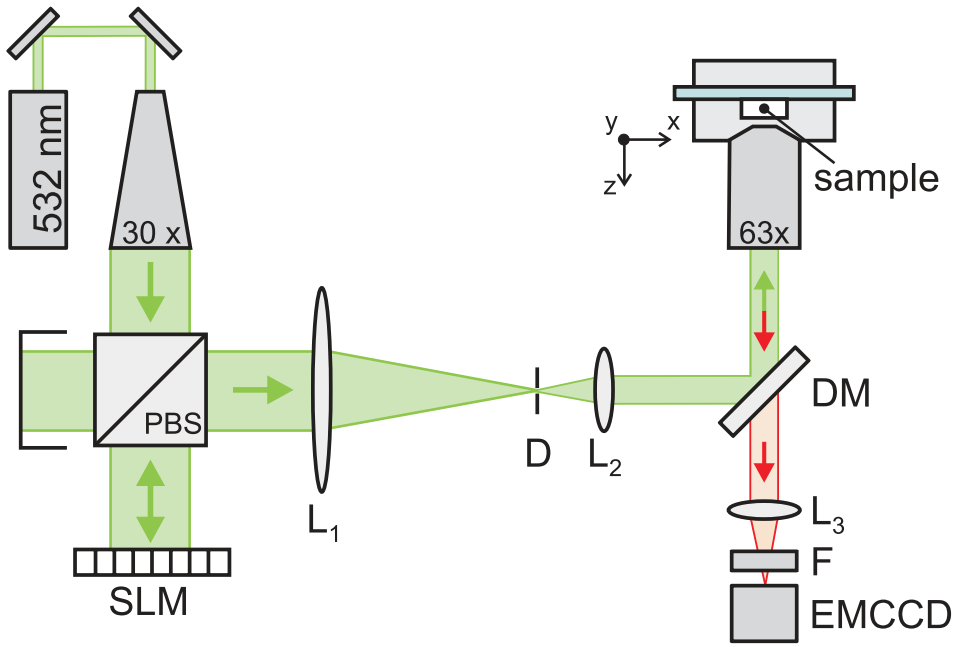

Fig. 5. Experimental setup. The left part consists of a laser (532 nm) that is expanded by a 30x beam expander and modulated with a spatial light modulator (SLM). A 1:2 demagnifying telescope images the SLM on the back aperture of a 63x microscope objective. The objective focuses the light on a sample that is mounted on a XYZ piezo positioning stage. A dichroic mirror (DM) and a bandpass filter (F) block the excitation light. The fluorescence emission is imaged on an electron multiplying CCD camera (EMCCD). D, iris diaphragm; PBS, polarizing beam splitter cube; L_1, L_2, L_3, lenses with a focal distance of 200 mm, 100 mm and 150 mm, respectively. Some folding mirrors and beam attenuation optics were omitted.

phase delays of $0, 2\pi/5, 4\pi/5, 6\pi/5$, and $8\pi/5$ and a sinusoid is fitted to these measurements. Before advancing to the next segment, the phase delay is reset to 0.

A.2. Measurement sequence

Channel demixing is achieved by measuring the propagation coefficients from the incident channels towards the embedded target. After all propagation coefficients are measured, it is known which linear combination of scattering channels focuses at the target. To quantify the effectiveness of this method, we measure the intensity at the probe position before and after the demixing procedure.

Since the field inside the medium is a completely random speckle pattern, the initial intensity is a random variable. A single measurement will not provide a reliable reference. Therefore, we measure the speckle averaged initial intensity I_0 by generating 500 different random combinations of incident channels and determining the average fluorescence intensity. This way, fluctuations caused by volume speckle are averaged out and a reliable measure for the initial intensity is found.

Next, the propagation constants for the different scattering channels are measured. This measurement takes approximately 18 minutes. During these measurements, the dye in the sphere photobleaches, which causes the response of the probe to decrease. Since we are interested in how much excitation light is focused on the target position, we have to take into

#89796 - $15.00 USD Received 15 Nov 2007; revised 20 Dec 2007; accepted 21 Dec 2007; published 2 Jan 2008

account the reduced response of the probe particle

$$\eta_{\text{measured}} = \frac{I_{\text{opt}}}{I_0}\frac{I_1}{I_2}, \tag{1}$$

where I_{opt} is the fluorescence intensity directly after constructing the optimal combination of scattering channels. I_1 is the fluorescence intensity at the start of this measurement step (directly after the reference measurement), and I_2 is the intensity at the end of the measurements (directly before the SLM is programmed with the optimal configuration). The ratio I_1/I_2 - which is between 1.0 and 1.8 when the sample is positioned at a typical position and between 1.5 and 3.9 when the sample is positioned at the brightest speckle - corrects for the fact that photobleaching decreases the sensitivity of the probe.

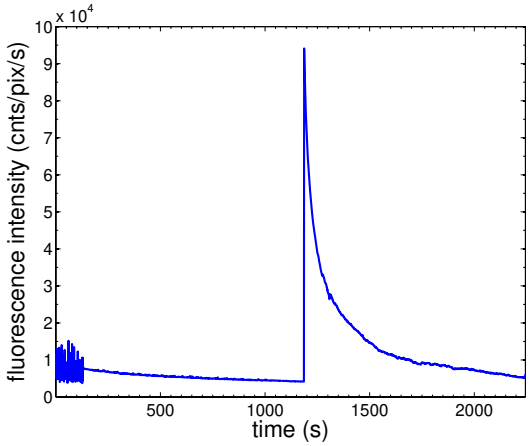

Fig. 6. Evolution of the fluorescence intensity during the measurements. The measurement procedure has three phases. 0-130 s, reference measurement; 130-1187 s, measurement of propagation coefficients; at 1187 s, construction of optimal wavefront; 1187-2244 s, fluorescence measurement with optimal wavefront.

Figure 6 shows how the fluorescence intensity evolves during the measurement sequence. During the reference measurement, the intensity fluctuates rapidly. In the next step, the propagation constants are measured. Since we only cycle the phase of a single channel at a time, the illuminating wavefront is practically constant. During this step the fluorescence intensity decreases slowly due to photobleaching. After the measurements have been performed for all segments, the phase modulator is programmed with the optimal phases and the fluorescence intensity jumps to a higher value as the incident light now interferes constructively at the target. After this jump, the wavefront is kept constant. The reason that the fluorescence intensity decreases is that the higher incident intensity on the sphere causes the dye to bleach more rapidly.

A.3. Sample preparation and characterization

We demonstrated how interference of scattered light was used to focus light deep inside disordered metamaterials. Our samples are strongly scattering, that is, the mean free path for light is of the order of the wavelength. Inside the sample, fluorescent probes mark the target positions. Typically, the probes are over 10 mean free paths deep, which makes it impossible to focus light on them using conventional means (Also see Sec. B.4). In this section we address the fabrication and characterization of these samples.

#89796 - $15.00 USD Received 15 Nov 2007; revised 20 Dec 2007; accepted 21 Dec 2007; published 2 Jan 2008

A.3.1. Sample preparation

Our samples consist of a layer of Zinc Oxide pigments (Aldrich Zinc Oxide $< 1\ \mu$m, 99.9%). The average particle diameter is 200nm (measured using scanning electron microscopy). The fluorescent probes are made from polystyrene and have a specified diameter of 300 ± 15 nm (Duke Scientific red fluorescent nanospheres dyed with FireFly^{TM}). An aqueous suspension of pigment and spheres was sprayed on a standard microscope cover slide using a commercial airbrush (Harder & Steenbeck Evolution). The thickness of the dried samples was measured with an optical microscope by making a scratch in the surface. The background fluorescence of the ZnO was shown to be negligible compared to the fluorescence of the dyed nanospheres.

A.3.2. Measurement of the mean free path

Transport of light in scattering media is quantified by the transport mean free path ℓ. A method for obtaining ℓ is to measure the total (diffuse) transmission of light using an integrating sphere. ℓ then follows from the relation [35]

$$\frac{1}{T} = \frac{L + z_{e1} + z_{e2}}{\ell + z_{e1}}, \tag{2}$$

where T is the total intensity transmission, L is the sample thickness and z_{e1}, z_{e2} are the extrapolation lengths that describe boundary effects on the front and back surfaces of the sample respectively. The extrapolation lengths follow from the effective refractive index of the medium, n_{eff} [36]. We measured the total transmission through a set of similar samples with varying thickness. The inverse total transmission for an ensemble of 14 samples is plotted in Fig. 7. The samples range in thickness from 6 μm to 32 μm. As expected, the inverse total transmission increases linearly with sample thickness. We obtain a good linear fit for $\ell = 0.7 \pm 0.2\ \mu$m and $n_{\text{eff}} = 1.4 \pm 0.1$. The extrapolation lengths can then be calculated from n_{eff} and we find $z_{e1} = 1.15 \pm 0.2\ \mu$m and $z_{e2} = 1.24 \pm 0.2\ \mu$m.

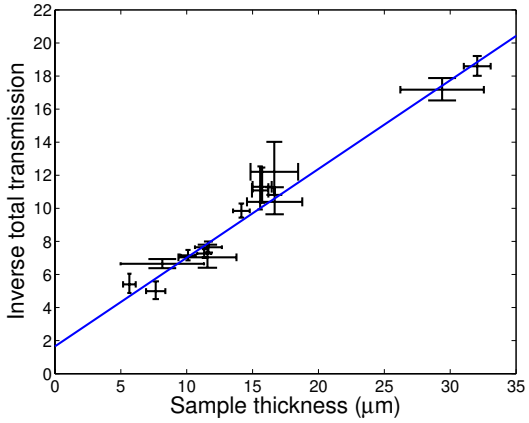

Fig. 7. Inverse total transmission through layers of ZnO pigment. The solid line is a fit of Eq. (2) with $\ell = 0.72\ \mu$m, $z_{e1} = 1.15\ \mu$m, and $z_{e2} = 1.24\ \mu$m. Error bars indicate the standard deviation of the measured thickness and total transmission at different positions on the sample.

A.3.3. Determination of the depth of the fluorescent probe

For each experiment we select a different probe sphere at a different depth inside a sample. To determine the depth of the probe, we image the diffuse spot of emitted light and fit this data with

#89796 - $15.00 USD Received 15 Nov 2007; revised 20 Dec 2007; accepted 21 Dec 2007; published 2 Jan 2008

diffusion theory. The accuracy methods that rely on inverting the diffusion equation is limited to about one mean free path due to noise [37].

The intensity inside a disordered medium with a source at depth z_0 follows from diffusion theory. We solved the diffusion equation for a slab of thickness L using the Dirichlet boundary conditions $I(-z_{e1}) = 0$, and $I(L+z_{e2}) = 0$ [38,39]. The extrapolation lengths z_{e1} and z_{e2} account for the reflections at the front and the back of the sample, respectively. A closed form solution is found using Fourier transformed traversal coordinates $\mathbf{q}_\perp \equiv (q_{\perp x}, q_{\perp y})$.

$$\tilde{I}_d(\mathbf{q}_\perp, z) = \begin{cases} J_{\text{in}} \frac{\sinh(q_\perp[L_e - z - z_{e1}])\sinh(q_\perp[z_0 + z_{e1}])}{D q_\perp \sinh(q_\perp L_e)} & z > z_0 \\ J_{\text{in}} \frac{\sinh(q_\perp[L_e - z_0 - z_{e1}])\sinh(q_\perp[z + z_{e1}])}{D q_\perp \sinh(q_\perp L_e)} & z \leq z_0 \end{cases} \tag{3}$$

where $\tilde{I}_d$ is the diffuse energy density at depth z, $q_\perp \equiv \sqrt{q_{\perp x}^2 + q_{\perp y}^2}$, and J_{in} is the power of the source in Watts. D is the diffusion constant and $L_e \equiv L + z_{e1} + z_{e2}$.

To obtain the depth of the source, we Fourier transform the microscope image of the fluorescence light and fit Eq. (3) with z=0 using z_0 and an intensity prefactor as fit parameters.

A.4. 3D scan results

Conventional focusing does not work in strongly scattering materials such as our samples. The absence of a ballistic focus was confirmed by performing an extensive 3-dimensional scan of the sample with respect to the microscope objective. The fluorescence emission strongly fluctuates with the sample position. These fluctuations are the result of a volume speckle field in the medium that is formed by scattered monochromatic light. As the sample moves, the volume speckle fluctuates randomly. For each depth of the geometrical focus, we record the brightest speckle intensity. Figure 8 shows the results of a typical 3-D scan. The depth of the geometrical focus was estimated to be $n_{\text{eff}}z$, with $n_{\text{eff}} = 1.4$ as measured, and z the position of the translation stage. No sign of a ballistic focus was observed. In other words, it is not possible to focus light on the target using conventional means.

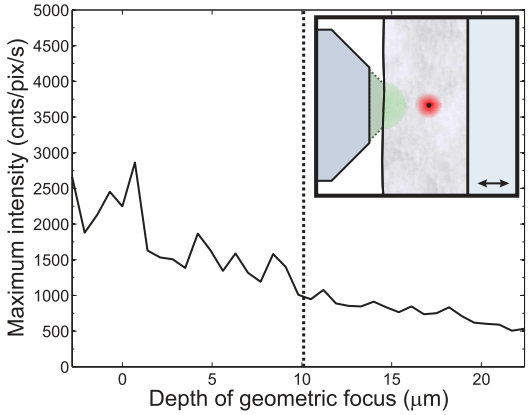

Fig. 8. Determination of the absence of a geometrical focus. The sample is moved with respect to the objective (inset). For each depth, the sample is scanned in a plane parallel to the surface to find the maximum fluorescence intensity (solid line). In homogeneous media, there would be a sharp peak at the point where the fluorescent sphere is in the geometrical focus of the microscope objective (dotted line). In disordered photonic media, a geometric focus cannot be formed. The highest intensity is found when 'focusing' just below the sample surface.

#89796 - $15.00 USD Received 15 Nov 2007; revised 20 Dec 2007; accepted 21 Dec 2007; published 2 Jan 2008

B. Analysis of the channel demixing method

The optical field E at a point $\mathbf{r}_b$ inside the medium is given by

$$E(\mathbf{r}_b) = \int g(\mathbf{r}_b, \mathbf{r}_a) \mathscr{S}(\mathbf{r}_a) d^3\mathbf{r}_a, \tag{4}$$

where g is Green's function for propagating from the sources $\mathscr{S}(\mathbf{r}_a)$ to point $\mathbf{r}_b$. In a disordered medium, g is stochastic and, therefore, initially unknown. We treat each segment of the phase modulator as a sheet source with amplitude A and phase ϕ. Since the phase modulator is in good approximation illuminated homogeneously, all amplitudes A are equal. By integrating over the surface area S of each of the N segments, Eq. (4) is discretized,

$$E(\mathbf{r}_b) = \sum_a^N \int_{S_a} g(\mathbf{r}_b, \mathbf{r}_a) d^2\mathbf{r}_a A e^{i\phi_a}, \tag{5}$$

$$\equiv A \sum_a^N g_{ba} e^{i\phi_a}. \tag{6}$$

When the phase of a single segment a of the phase modulator is changed, the intensity at point $\mathbf{r}_b$ responds as

$$I(\mathbf{r}_b) \equiv |E(\mathbf{r}_b)|^2 = I_{0b} + 2A\mathrm{Re}(E^*_{b\bar{a}} g_{ba} e^{i\phi_a}), \tag{7}$$

with

$$I_{0b} \equiv |E_{b\bar{a}}|^2 + A^2 |g_{ba}|^2, \tag{8}$$

$$E_{b\bar{a}} \equiv A \sum_{a' \neq a}^N g_{ba'} e^{i\phi'_a} \approx E(\mathbf{r}_b), \tag{9}$$

Since the number of segments N is large, $E_{b\bar{a}} \approx E(\mathbf{r}_b)$ and, therefore, equal for each of the segments. By repeating this procedure for all segments a, we measure the coefficients g_{ba} up to an unknown common prefactor $E(\mathbf{r}_b)$.

Once all coefficients g_{ba} are known, our channel demixing method maximizes $E(\mathbf{r}_b)$ by setting $\phi_a = -\arg(g_{ba})$ for all segments. This configuration of phases gives the global maximum of Eq. (6),

$$E_{\max}(\mathbf{r}_b) = A \sum_a^N |g_{ba}|. \tag{10}$$

A comparison with Eq. (6) shows that now all amplitudes are summed with the same phase and that all incident channels will interfere constructively at the target.

B.1. Maximum relative intensity enhancement - scalar waves, simplified case

The theoretical increase in intensity that can be achieved with channel demixing depends on the number of modulator segments N and the statistical properties of coefficients g_{ba}. In disordered systems it is often allowed to assume that the coefficients are independently drawn from a single circular Gaussian distribution [12, 13, 40–42]. Under this assumption, the expected ratio between the original diffuse intensity and the maximally achievable intensity equals

$$\eta = \frac{\pi}{4}(N-1) + 1. \tag{11}$$

#89796 - $15.00 USD Received 15 Nov 2007; revised 20 Dec 2007; accepted 21 Dec 2007; published 2 Jan 2008

where N can never exceed the number of mesoscopic scattering channels. The number of contributing scattering channels depends on the depth of the target. The deeper the target is embedded in the scattering material, the more channels will contribute to the mixing process. We estimate the number of channels that contribute to the target field by examining the size of the diffuse spot of the fluorescence light. The number of scattering channels in a spot with surface area A is given by [43, 44] $N_{\max} = 2\pi A/\lambda^2$. In Fig. 3(b), the full width at half maximum of the diffuse spot is 15 μm, which leads to $A = 177\ \mu\mathrm{m}^2$ and $N_{\max} = 3.9 \cdot 10^3$. In our our experiment $N = 640 \ll 3.9 \cdot 10^3$ and neighboring segments were uncorrelated.

B.2. Maximum relative intensity enhancement - finite size probe

Ideally, the sphere that is used as a probe is only sensitive to the field of a single polarization at a single point. In reality, however, the fluorescent sphere probes the summed intensity of three polarizations in a finite volume. Therefore, it is as if we have multiple targets for which we try to increase the intensity simultaneously. As a result, the extra intensity is divided over all targets. The ratio between the original diffuse intensity and the maximally achievable intensity now equals

$$\eta_{\mathrm{M}} = \frac{\pi}{4}\frac{N-1}{M} + 1, \tag{12}$$

where M is the number of targets. We determine M by calculating how many orthogonal fields can exist in the volume of the probe sphere. Using Mie theory we find that for spheres of 300 ± 15 nm the three electric dipole modes and the three magnetic dipole modes all give an equally strong contribution to the fluorescence power. The sphere is too small to support higher order (quadrupole) modes, so we estimate that the probe contains 6 optical modes. Using Eq. (12) with $M = 6$ and $N = 640$, we find an expected theoretical enhancement of 85. The experimental enhancement was approximately 25% of this value. We believe that the most important reason for not reaching the theoretical maximum enhancement is photobleaching. The channel demixing method favors the mode that initially is the brightest. Unfortunately, this target mode also photobleaches the fastest. Since we correct only for the average photo bleaching rate (See Section A.2), the measured enhancement will systematically be lower than the actual enhancement.

B.3. Maximum relative intensity enhancement of speckle scan

When the sample is moved, the speckle pattern in the medium fluctuates. As a result, the probe fluorescence will fluctuate too. Therefore, when a 3D-scan of the sample position is performed, at some points the intensity will be somewhat higher than the diffuse background. We used numerical simulations to calculate the expected maximum enhancement that this scanning technique can achieve. We assumed Rayleigh statistics for the speckle field and calculated the summed intensity in 6 independent optical modes at N_r different positions. The simulation was repeated 1000 times and for each run the maximum speckle intensity was stored. The number of independent speckles, N_r, is limited by the diffuse intensity envelope of the light inside the material. We estimate that N_r is between 1000 and 10000, depending on the depth of the probe. With these numbers, the simulations predict that the brightest speckle is 2.9 to 3.4 times as intense as the diffuse background.

B.4. Calculation of diffuse and ballistic intensities inside the medium

B.4.1. Diffuse intensity

When a slab of diffusive material is illuminated, the incident light can be described by a diffuse source at depth $z_0 = \ell$ in the medium [45]. The maximum diffuse intensity at depth z is found

#89796 - $15.00 USD Received 15 Nov 2007; revised 20 Dec 2007; accepted 21 Dec 2007; published 2 Jan 2008

by inverse Fourier transforming (3) with $x = y = 0$.

$$I_d(x=0,y=0,z) = \frac{1}{2\pi}\int_0^\infty \tilde{I}_d(q_\perp,z)S(q_\perp)q_\perp dq_\perp. \tag{13}$$

Where $S(q_\perp)$ accounts for the spatial extent of the source. We modelled the source as a Gaussian spot that encompasses 640 scattering channels; $S(q_\perp) = \exp(-q_\perp^2/0.43)$. Eq. (13) was evaluated numerically. The diffuse intensity was used to normalize the theoretical curve for the perfect ballistic intensity in Fig. 4.

B.4.2. Perfect ballistic intensity

We assume that all geometrical abberations are perfectly corrected and that all the incident light is directed towards a sphere in the geometrical focus. While travelling through the disordered medium, scattering and diffraction on sub-wavelength structures attenuate the incident beam according to the Lambert-Beer law,

$$I_b = \frac{e^{-z/\ell_{sc}}}{Av}, \tag{14}$$

where I_b is the ballistic energy density at the sphere, A is the cross-section area of the sphere, z is the depth of the sphere, v is the velocity of light inside the medium and ℓ_{sc} is the scattering mean free path for light. The parameters ℓ_{sc} and v have not been measured directly for our samples. We can, however, give an upper limit for the ballistic intensity by overestimating $\ell_{sc} = \ell$ and underestimating $v = 3D/\ell$. The ballistic intensity was normalized by the diffuse intensity and plotted in Fig. 4.

Acknowledgment

We thank Prof. Willem Vos for valuable discussions. This work is part of the research program of the "Stichting voor Fundamenteel Onderzoek der Materie (FOM)", which is financially supported by the "Nederlandse Organisatie voor Wetenschappelijk Onderzoek (NWO)".

#89796 - $15.00 USD Received 15 Nov 2007; revised 20 Dec 2007; accepted 21 Dec 2007; published 2 Jan 2008